IAC-17,C4,3,3,x38219

PLUME FLOW FIELD ANALYSIS FOR LANDER PROPULSION SYSTEM OF CHANDRAYAAN-2 MISSION

Abhishek Sharma[a*], Deepak Kumar Agarwal[b], J. C. Pisharady[c], S. Sunil Kumar[d]

[a] *Indian Space Research Organization (ISRO), India, abhisheksharma@lpsc.gov.in*
[b] *Indian Space Research Organization (ISRO), India, dagarwal_iitk@yahoo.com*
[c] *Indian Space Research Organization (ISRO), India, jc_pisharady@lpsc.gov.in*
[d] *Indian Space Research Organization (ISRO), India, s_sunilkumar@lpsc.gov.in*
**Corresponding Author*

Abstract

The upcoming Chandrayaan-2 mission of ISRO is planned to deploy a lunar lander and rover on a specified lunar site. The mission objective is to ensure a safe and soft landing of lander module on the lunar surface. The lander-craft will be released from lunar orbit, which will further undergo various lunar bound phases like de-boosting, rough braking, precision braking, and vertical descent. Chandrayaan-2 lander will employ a clustered configuration of 800N engine along with 50N attitude control thrusters placed at the bottom of spacecraft, to decelerate the spacecraft for braking and soft landing on lunar surface. The engines will be operated together in different phases to reduce spacecraft's velocity to move from 100km North Pole to 6km South Pole lunar altitude location. The thermal environment near the thruster varies substantially when all thrusters will be operated simultaneously to decelerate the lander during de-boost and initial braking phase. The thermal protection system for lander will be designed to maintain the temperature of lander-craft systems within the safe limits during this phase. The simultaneous firing of all four engines can result in possible interaction of thruster plumes and flow reversal, which will eventually lead to higher thermal loads on spacecraft structures. Plume may also impinge on the lander legs resulting in higher convective heat load on leg surfaces. In order to study multiple engine plume effects and to determine thermal load on lander craft structures, a detailed numerical study is carried out for lander propulsion system in near vacuum condition. Navier Stokes Solver coupled with radiative transport equation (RTE) is used to study multiple engine plume interactions, reverse flow characteristics, plume impingement and for estimation of convective and radiative thermal load on lander structures. The study highlights the plume flow field for the clustered engine configuration of Chandrayaan-2 lunar lander and provides input to design thermal protection system for lander to sustain harsh thermal environments due to multiple engine firing.

Keywords: Chandrayaan-2,clustered, plume, thermal

Nomenclature

ρ	density, kg/m^3
$\vec{v}$	velocity vector, m/s
p	pressure, Pa
e_t	total energy, J/kg
τ_{eff}	effective viscous stress tensor, N/m^2
λ_{eff}	effective thermal conductivity, W/mk
A	area vector
a	absorption coefficient
Cp	specific heat at constant pressure
Ckω	cross-diffusion term for k-ω turbulence model
D	(Hydraulic) diameter, m
e	specific energy,J/kg
h	enthalpy,J/kg
l	length, m
M	Mach number
T	Temperature,K
x	Coordinate in x direction
y	Coordinate in y direction
z	Coordinate in z direction
ρ	Density,kg/m3
σ	Stress tensor
u	Velocity,m/s
μ	Viscosity,Ns/m2
γ	Ratio of specific heats
I	radiation intensity
$\vec{r}$	position vector
$\vec{s}$	direction vector
s	path length
n	refractive index
σ_s	scattering coefficient
σ	Stefan-Boltzman constant
$\emptyset$	phase function
Ω'	solid angle

1. Introduction

The success of Chandrayaan-I mission gave impetus to ISRO to embark on an advanced mission to explore Moon in greater depth. Currently, ISRO is finalising Chandrayaan-2 mission which will deploy lander and rover on surface of the moon. The lunar lander will soft land on a specified site and will release the 8 wheeled rover for an in situ experimentation. Figure 1 displays the lander model with engines placed at bottom and rover attached to the slider.

Chandrayaan-2 mission will employ clustered configuration of engines for lunar lander to decelerate the spacecraft for soft landing on lunar surface. The lander-craft will be released from lunar orbit, which will further undergo various lunar bound phases like de-boosting, rough braking, precision braking, and vertical descent. The clustered engines will be operated together in de-boosting and rough braking phase to reduce spacecraft's velocity to move from 100 km North Pole to 6 km South Pole altitude location. Figure 2 shows the landing sequence highlighting the duration of simultaneous firing of all four 800N engines.

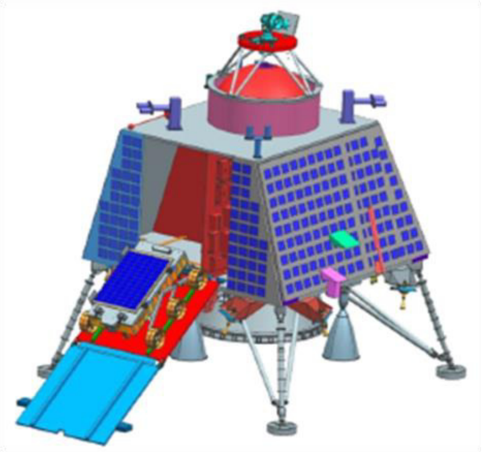

Fig.1: Chandrayaan-2 Lander Model

All 800N engines will operate for considerable amount of time imposing maximum heat load on lander structure. The simultaneous firing of all four engines can result in possible interaction of thruster plumes and flow reversal, which will eventually lead to higher thermal loads on spacecraft structures. Plume may also hit the lander legs resulting in higher convective heat load on leg surfaces. It is necessary to understand flow field of multiple engines operating in vacuum and to determine the reverse flow characteristics for accurate guidance of landercraft.

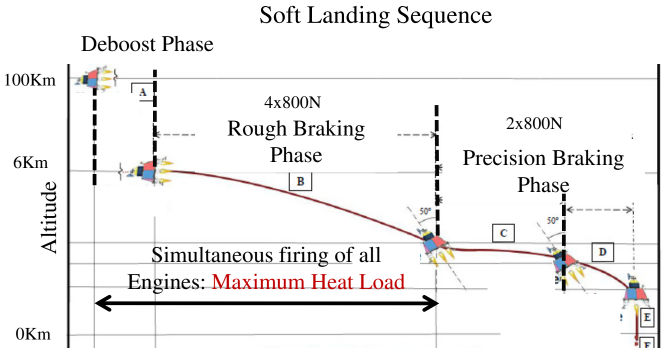

Fig.2: Chandrayaan-2 Landing Sequence

Base flow field at high altitudes within the earth's atmosphere is characterised by highly coupled, unsteady and complex flow features.Figure 3 displays the base heating flow features as mentioned in study carried out by Mehta et al [1]. It shows the formation of updraft flow due to plume-plume interactions. The updraft plume is seen to form stagnation region between the engines which will impose high convective heat loads.Differences are expected in lunar ambience but this flow field still serves as a standard reference. Nallasamy R [2] has also studied the base flow and heat transfer characteristics for four nozzle clustered engine. Wang et al [3] has done CFD investigation for base flow field for a four-engine clustered configuration. The research study captured qualitative base flow features which were found to be in good agreement with experimental observations. Limited numerical and analytical studies have been conducted to fully characterize multi-plume base heating.

Moreover, the above mentioned studies for clustered operation of engines were not done for highly under expanded conditions, which will be the case for operation of Chandrayaan-2 lander engines. Moreover, it is imperative to determine heat load on lander structure during multiple firing of engines, which will be used to design thermal protection of lander.

In order to study plume field characteristics and to estimate radiative and convective heating of spacecraft during simultaneous operation of engines, an integrated three-dimensional CFD model of Chandrayaan-2 lander was developed.

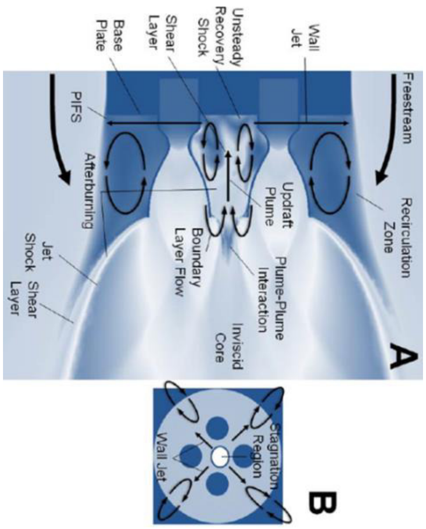

Fig.3: Base heating flow features [1]

2. CFD Modelling

2.1 Physical Model

The 3D schematic of Chandrayaan-2 lander used for analysis is shown in Figure.4. It shows the different elements of lander considered for CFD study.

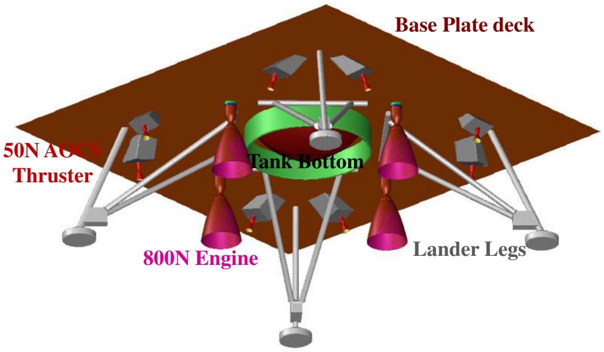

Fig.4: 3D schematic of CFD model

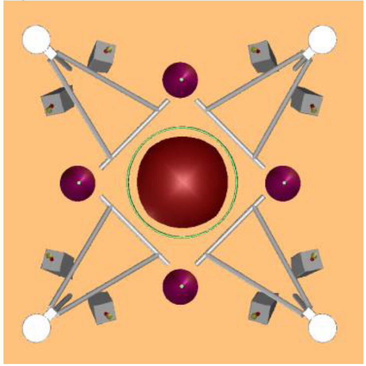

Fig.5: Bottom View of Lander

The lander CFD model was developed considering bottom deck, 800N engines, 50N AOCS thrusters, lander legs, tank bottom and 50N thruster brackets. Figure 5 shows the bottom view of lander which clearly indicates the location of 800N and 50N engines at bottom deck

2.2 Computational domain & boundary conditions

Figure 6 shows the computational domain and boundary conditions used for the CFD analysis. Owing to the symmetry in the geometry, a 45deg. sector, with two plane symmetry consisting of half 800N thruster nozzle, one 50N AOCS, bracket and lander leg is considered for analysis.
Pressure inlet condition and total temperature is applied at thruster nozzle inlet. Constant temperature with no slip wall boundary condition is imposed at base plate, lander legs and AOCS structure walls. NASA-CEA program is used for obtaining properties of combustion gas at a mixture ratio of 1.66 (propellant combination of MMH and NTO) and chamber pressure of 7 bar. The density of combustion gas is modeled as ideal gas.

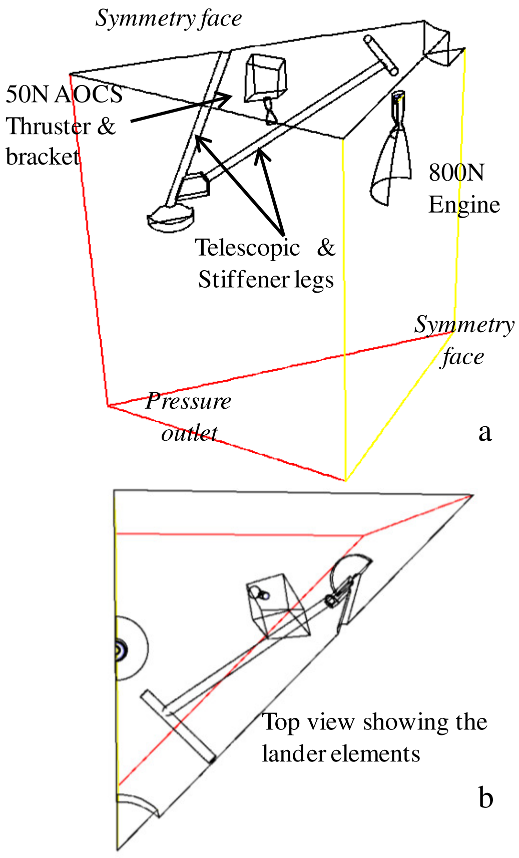
Symmetry face
50N AOCS Thruster & bracket
800N Engine
Telescopic & Stiffener legs
Symmetry face
Pressure outlet
a
Top view showing the lander elements
b

Fig.6 (a, b): Computational Domain & Boundary Conditions

A combination of structured and unstructured grid with boundary (prism) layers near to bottom deck and lander legs was generated using ANSYS meshing. An attempt has been made to keep 10 grid points within boundary layer in order to capture near wall physics. In order to simulate high degree of under expansion similar to lunar ambience, a very low pressure condition was imposed at outlet boundaries. The CFD simulation for prediction of flow features and to estimate thermal load on lander structures is done within continuum valid region. Compressible Reynolds averaged Navier stokes equation (RANS) is used for flow modelling, with two equation SST-k-ω model for turbulence closure. Radiation modelling is carried out using the Discrete-Ordinates (DO) model which considers surface as well as gas radiation.

2.3 Governing equations

Navier-Stokes equations of mass continuity, momentum, energy are given as:

Continuity equation is gas phase:

$$\frac{\partial \bar{\rho}}{\partial t}+\frac{\partial \bar{\rho}\tilde{u}_j}{\partial x_j}=0 \qquad (1)$$

Momentum equation: The momentum balance for gas phase is written as:

$$\frac{\partial \bar{\rho}\tilde{u}_i}{\partial t}+\frac{\bar{\rho}\tilde{u}_j\tilde{u}_i}{\partial x_j}= -\frac{\partial \bar{p}}{\partial x_i}+\frac{\partial}{\partial x_j}\left(\tilde{\tau}_{ij}-\overline{\rho u_i'' u_j''}\right) \qquad (2)$$

Where $\tilde{\tau}_{ij}$ is a shear stress term given by;

$$\tilde{\tau}_{ij}=\mu\left(\frac{\partial \tilde{u}_i}{\partial x_j}+\frac{\partial \tilde{u}_j}{\partial x_i}\right)-\frac{2}{3}\mu\frac{\partial \tilde{u}_k}{\partial x_k}\delta_{ij} \qquad (3)$$

$\overline{\rho u_i'' u_j''}$ is a Reynolds stress term given by;

$$-\overline{\rho u_i'' u_j''}=\mu_t\left(\frac{\partial \tilde{u}_i}{\partial x_j}+\frac{\partial \tilde{u}_j}{\partial x_i}\right)-\frac{2}{3}\mu_t\frac{\partial \tilde{u}_k}{\partial x_k}\delta_{ij}-\frac{2}{3}\bar{\rho}k\delta_{ij} \qquad (4)$$

Energy equation: The energy balance for gas phase is written as:

$$\frac{\partial}{\partial t}\left(\bar{\rho}\widetilde{H}-\bar{p}\right)+\frac{\partial}{\partial x_j}\left(\bar{\rho}\tilde{u}_j\widetilde{H}\right)= \frac{\partial}{\partial x_j}\left[\left(\frac{\mu}{Pr}+\frac{\mu_t}{Pr_t}\right)\frac{\partial \tilde{h}}{\partial x_j}\right]+ \frac{\partial}{\partial x_j}\left[\tilde{u}_j(\mu+\mu_t)\left(\frac{\tilde{u}_i}{x_j}+\frac{\tilde{u}_j}{x_i}-\frac{2}{3}\frac{\partial \tilde{u}_k}{\partial x_k}\delta_{ij}\right)\right]+ \frac{\partial}{\partial x_j}\left[\left(\mu+\mu_t\sigma_k\right)\frac{\partial k}{\partial x_j}\right] \qquad (5)$$

2.3.1 Turbulence Closure

Two equation RANS model, SST k-ω is used for turbulence closure. SST k-ω model is widely used for industrial and research problems, as it uses the blending function which activates the k-ω formulation to model near wall flows and k-ε model to simulate flows away from wall. Turbulent viscosity is redefined to account for transport of turbulent shear stress. Equations for turbulent kinetic energy and turbulent dissipation equation are given below by equation (6) and (7) respectively.

Turbulent Kinetic Energy (TKE-k) equation for gas phase is given as:

$$\frac{\partial}{\partial t}(\rho k)+u_l\frac{\partial}{\partial x_l}(\rho k)=R_{ij}\frac{\partial u_i}{\partial x_j}-C_\mu\rho\omega k+ \frac{\partial}{\partial x_j}\left[\left(\mu+\mu_t\sigma_k\right)\frac{\partial k}{\partial x_j}\right] \qquad (6)$$

Where, $R_{ij}= \mu_t\left(\frac{\tilde{u}_i}{x_j}+\frac{\tilde{u}_j}{x_i}\right)-\frac{2}{3}\mu_t\frac{\tilde{u}_k}{x_k}\delta_{ij}-\frac{2}{3}\bar{\rho}k\delta_{ij}$ which is the turbulent stress tensor term.

Specific Dissipation Rate (SDR-ω) equation for gas phase is given as:

$$\frac{\partial}{\partial t}(\rho\omega)+\mu_l\frac{\partial}{\partial x_l}(\rho\omega)=\frac{\gamma}{\nu_t}R_{ij}\frac{\partial u_i}{\partial x_j}-\beta\rho\omega^2+ \frac{\partial}{\partial x_j}\left[\left(\mu+\mu_t\sigma_\omega\right)\frac{\partial \omega}{\partial x_j}\right]+2(1-F_1)\rho\sigma_{\omega 2}\frac{1}{\omega}\frac{\partial k}{\partial x_j}\frac{\partial \omega}{\partial x_j} \qquad (7)$$

Where, $F_1$is a blending function given as;

$$F_1=tanh\left[\left(min\left(max\left(\frac{\sqrt{k}}{0.09\omega y},\frac{500\nu}{y^2\omega}\right),\frac{4\rho\sigma_{\omega 2}k}{CD_{k\omega}y^2}\right)\right)^4\right]$$

And$CD_{k\omega}$ is a cross diffusion term given as, (8)

$$CD_{k\omega}=max\left(2\rho\sigma_{\omega 2}\frac{1}{\omega}\frac{\partial k}{\partial x_j}\frac{\partial \omega}{\partial x_j},10^{-20}\right)$$

2.3.2 Radiation Modelling

The radiation phenomenon was modelled using the Discrete Ordinates (DO) Model, which is applicable in diverse range of problems involving radiative heat transfer. The DO model is used to consider both surface to surface radiation, along with participation from gas. Radiative Transport Equation (RTE) is the governing equation of DO model. The RTE in form of a transport equation is shown below.

$$\nabla.\left(I\left(\left(\overrightarrow{r,s}\right)\right)\vec{s}\right)+(a+\sigma_s)I\left(\overrightarrow{r,s}\right)=an^2\,\frac{\sigma T^4}{\pi}+ \frac{\sigma_s}{4\pi}\int_0^{4\pi}I\left(\overrightarrow{r,s}\right)\emptyset\left(\left(\overrightarrow{s,s}\right)d\Omega'\right. \qquad (9)$$

In typical problems of gas emanating from rocket nozzle into very low pressure ambience, the major source of radiation is surface to surface, generally from high temperature rocket nozzle. In order to consider both direct surface radiation and gas radiation, appropriate input parameters were provided as required for solving RTE. In order to consider contribution of gas radiation, absorption coefficient, a as calculated in validation studies performed on small thrusters operating vacuum chamber was used. It was noticed that absorption coefficient being as function of partial pressure of constituent gases becomes very low in vacuum conditions. The scattering of gas assumed to be negligible and was not included for analysis.

The above governing equations are solved using finite volume methodology (FVM) in ANSYS FLUENT. Coupled scheme is used for pressure velocity coupling. Second order upwind scheme is adopted for discretization of pressure, momentum and energy equation. The iterative solution loop is performed until pre-set convergence criterion of energy equation and other residuals is below 10^{-8} and 10^{-5} respectively.

3. Results & discussion

Three-dimensional steady state analysis for Chandrayaan-2 lander mission is carried out to determine possibility of interaction between thruster plumes, flow reversal phenomenon and consequent radiative and convective heating of the lander structures.

3.1 Flow Physics

Figure7 shows the Mach number contours at symmetry plane between two engines. The maximum value of Mach number observed is 6.33 at the domain end, which is due to continuous expansion of plume into very low ambient pressure. It is observed that plume coming out of thruster interacts with each other at its periphery and interaction is observed to initiate at an axial location of around 0.2 m from the thruster nozzle exit. Shear layer interaction and plume compression is observed at the interaction location.

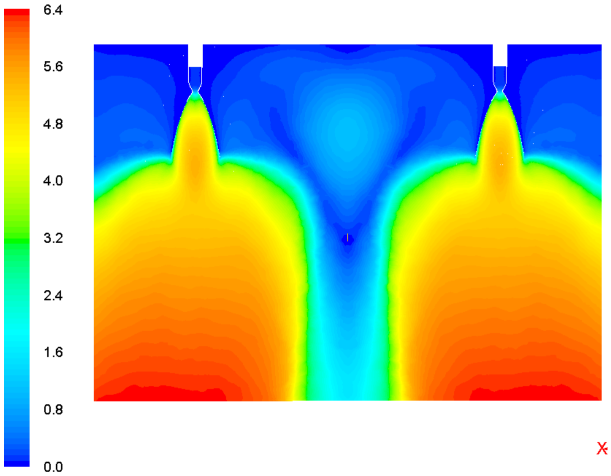

Fig.7. Mach contours at symmetry Plane

Figure 8 clearly presents Mach contour between the two engines at the symmetric plane. It shows the formation of entrainment region (low velocity zone) between the nozzles due to plume interaction.

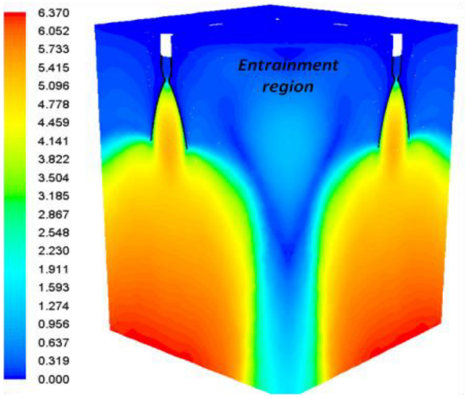

Fig.8. Mach contours at double symmetry Plane

Figure 9 shows the Mach vector contours with movement of updraft plume due to plume interaction of thrusters at the bottom. A sonic velocity flow is observed to move in upward direction, which eventually forms a recirculation zone between thruster nozzles.

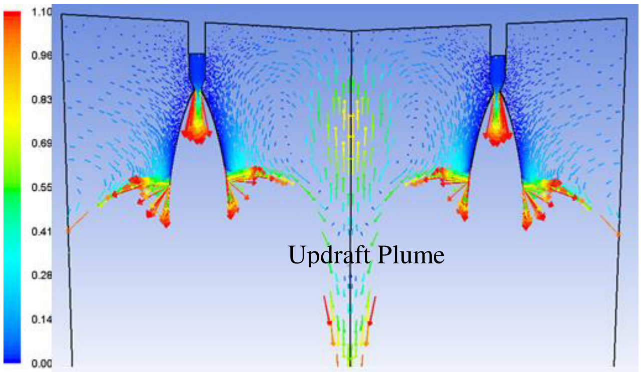

Fig.9. Vectors of Mach number for updraft plume,(m/s)

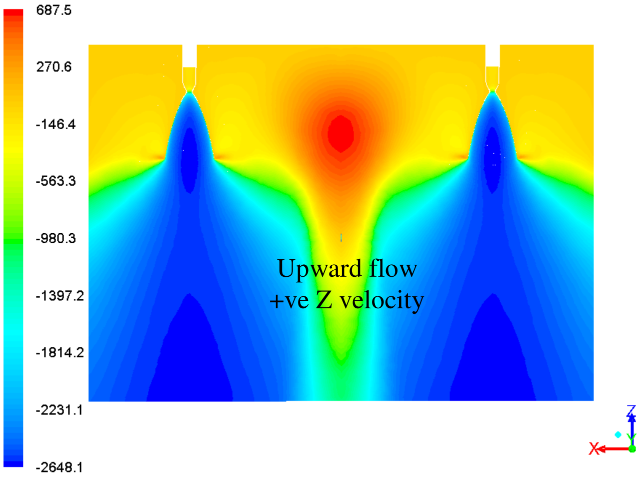

Fig.9. Z-velocity magnitude at symmetry plane,(m/s)

Figure 9 shows the presence of high upward Z-velocity region of 687m/s between the nozzles. Velocity zone of -146m/s is observed near the upward section of computational domain. Z-Velocity (m/s) plot shows formation of updraft plume with maximum velocity of 900m/s.

In order to understand the generation of updraft flow, static pressure at interaction zone was monitored. Figure 10 shows static pressure contour at symmetry plane. A high static pressure zone is seen to be created at the location of plume interaction, which has led to flow to move upwards up to base plate as seen in Fig.9.

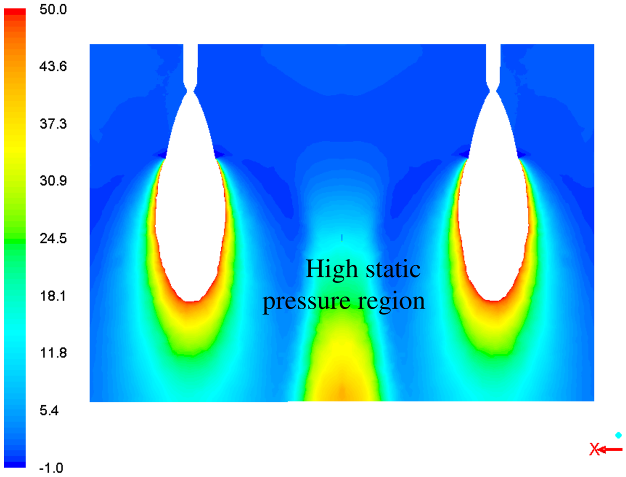

Fig.10. Static pressure profile at symmetry plane, (Pa)

Static pressure profile at cross-sectional (0.5m from nozzle exit) plane is displayed in Fig.11. It clearly shows a creation of high static pressure region at center due to multiple plume interaction. A low velocity zone created due to interaction of plumes has led to increase of static pressure at this location.

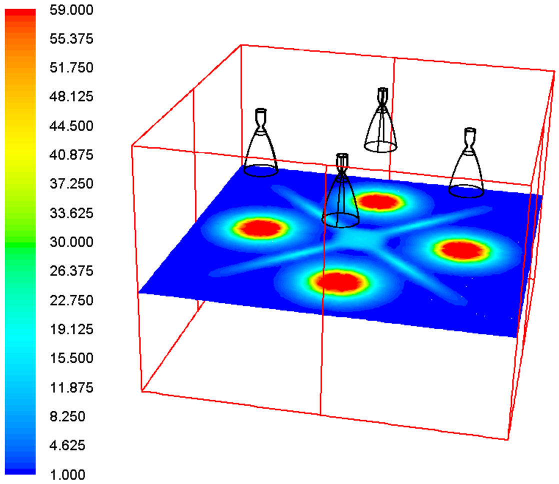

Fig11.Static pressure contour at cross-sectional plane, (Pa)

The intensity of updraft plume depends upon the static pressure rise at interaction location. A high density region will also appear between four thrusters, which is due to updraft & formation of high static pressure zone at multiple plume interaction area.

Turbulent kinetic energy (TKE) is the mean kinetic energy per unit mass associated with eddies in the turbulent flow, whereas turbulent Intensity is the measure of magnitude of RMS turbulent fluctuations in flow in comparison to mean flow velocity. TKE production happens due to fluid layer shearing and friction, which further dissipates as viscous forces at Kolmogorov scale. Figure 12 and 13 show the turbulent kinetic energy (TKE) and turbulent Intensity formation at the symmetric plane.

Figure 12 presents turbulent kinetic energy to decrease along the length of domain with maximum value at nozzle outlet. An increase in turbulent kinetic energy is seen at the interaction zone due to fluid layer shearing of multiple plumes. TKE production has also been seen between thruster nozzles and near the free stream boundary.

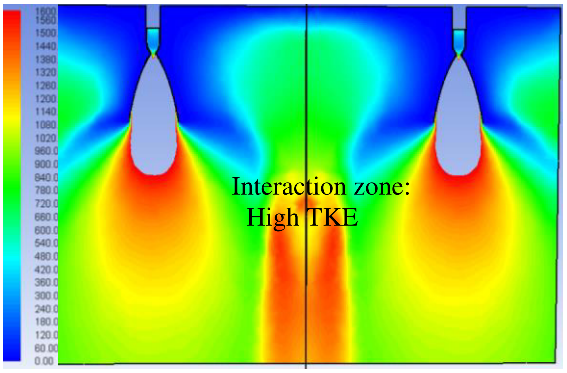

Fig.12.Turbulent kinetic energy contour at symmetry plane

Figure13 shows presence of higher turbulent intensity zone at plume-plume interaction and thruster nozzle outlet. Turbulent Intensity is high in nozzle divergent and varies along the axial direction, as the combustion gas expands into low pressure ambient. Mild turbulent intensity region is observed between thruster nozzles (entrainment region) which is due to formation of updraft plume.

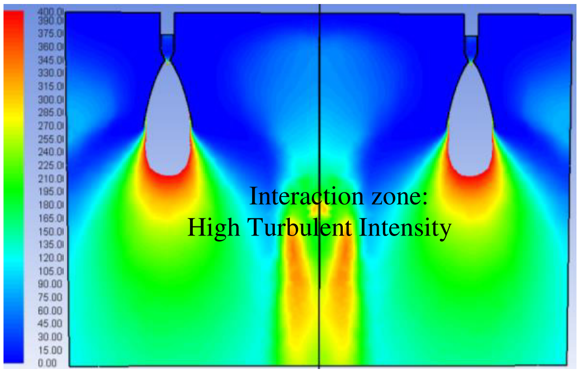

Fig.13. Turbulent Intensity contour at symmetry plane (%)

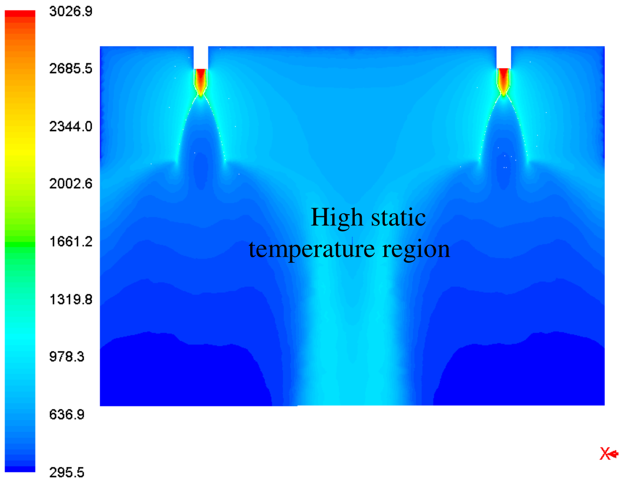

Fig.14. Temperature contour at symmetric plane,(K)

Figure14 shows static temperature distribution of plumes at symmetry plane between nozzles. The high temperature gas cools down due to expansion as it comes out of the nozzle. A high temperature zone is seen at nozzle throat and at plume interaction zone. Temperature increases due to shearing and slowing down of gas plume at periphery down of gas plume at periphery down of gas plume at periphery.

A high temperature zone at plume interaction zone and near nozzle throat area is observed. Temperature at interaction zone on plume boundary is seen to be around 1000 K. This high temperature static zone at the interaction of thruster plume would serve as the main source of radiation and can result in heating of the base plate and Lander assembly.

A density Iso-surface (1.5e-05 kg/m^3) mapped with temperature is shown in Fig. 15. The 3D plot shows the plume temperature and a formation of high temperature zone at the interaction region.

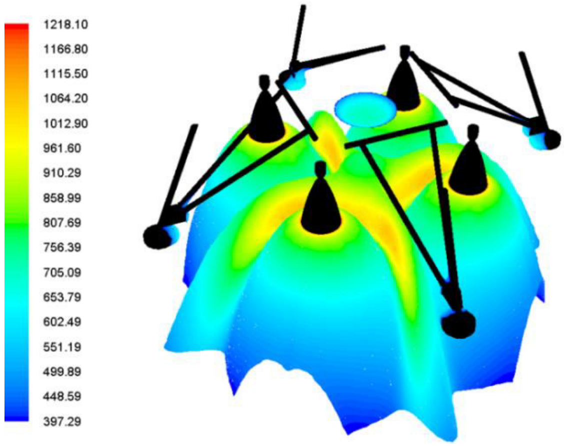

Fig.15 .Density Iso Surface: Static temperature 3D map (1.5e-05 kg/m^3)

Figure 16 shows the temperature profile at a cross-section plane, (0.5m from nozzle exit) of computational domain.

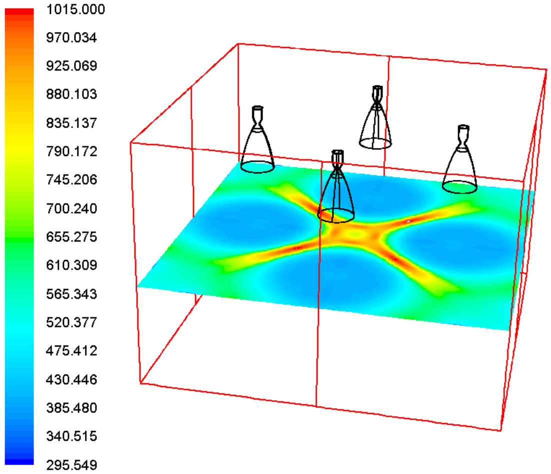

Fig.16. Temperature profile at cross-sectional plane-3D view, (K)

It shows formation of high static temperature region at center and plume periphery due to multiple plume interaction. The remaining portion of bottom plane exists at lower temperature due to plume expansion into vacuum.

Figure17 presents velocity vector plot for interacting plumes colored by static temperature. Velocity vectors show that, major portion of gas exiting from the nozzles is going downward along the axial direction. A high temperature updraft plume with temperature around 705K is seen to move in upward direction up to base plate. A recirculating gas pocket is seen to form between the nozzles and base plate segment. This entrapped gas moves upward and recirculates between thruster nozzles. The movement of high temperature gas in this entrainment zone would lead to convective heating of base plate deck and AOCS structure.

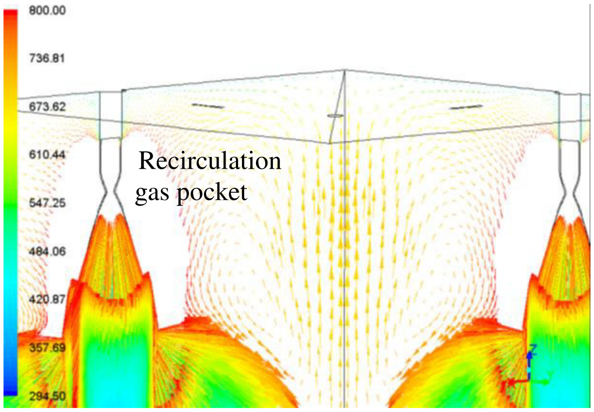

Fig.17.Vector plot for static temperature in entrainment zone, (m/s)

3.2 Heat Flux Estimation for Chandrayaan-2 Lander

Chandrayaan-2 spacecraft will experience maximum radiative and convective heat load during simultaneous operation of thrusters. In order to estimate thermal load on lander in this regime, radiative and convective heat fluxes over spacecraft structures are separately calculated and are reported below.

3.2.1 Radiative Heat Flux Estimation

Radiative heating of lander base plate and lander structure is estimated using discrete ordinate radiation model. Surface incident radiation, which is total incident flux coming onto the walls is estimated and presented below. Figure 18 shows surface incident radiative heat flux at base plate. A localized heating of base plate is observed near the 800N engine nozzle inlet. Maximum surface incident radiation is seen near the thruster inlet, which is primarily due to high temperature nozzle throat.

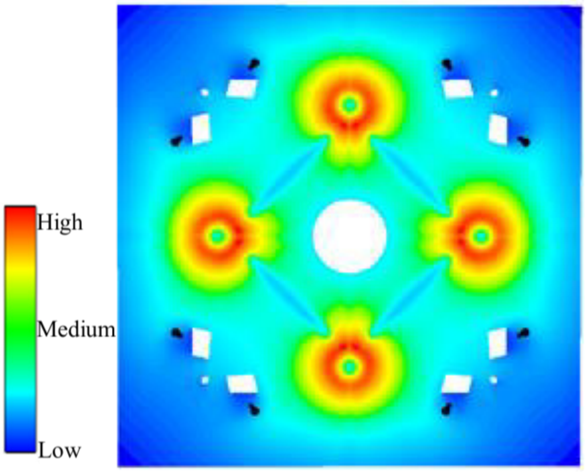

Fig.18. Surface incident radiation contour of lander assembly-baseplate, (W/m^2)

Figure 19 shows the bottom view for surface incident radiation on lander legs structure. It shows higher value of incident flux at leg surfaces facing plume and high temperature thruster nozzles directly.

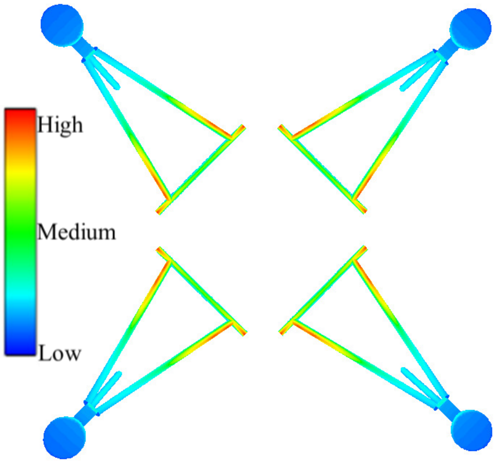

Fig.19. Surface incident radiation contour of lander assembly, (W/m^2)

Figure 20 shows the surface incident radiative heat flux at 50N bracket structure. A larger heating of bracket base is observed at centre portion with maximum surface incident radiative flux. The localized heating of bracket near thrusters is due radiative heating from high temperature nozzle surface.

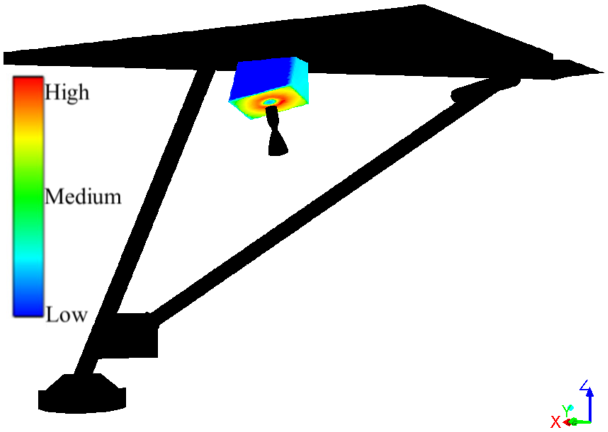

Fig.20. Surface incident radiation contour for 50N bracket, (w/m^2)

Surface incident radiation flux on tank bottom as calculated in CFD model is displayed in Figure 21. It shows intensity of surface incident load on tank bottom surface along with lander leg and nozzle structure. Maximum surface incident load was observed bottom part of tank surface, which is directly exposed to high temperature nozzle surface.

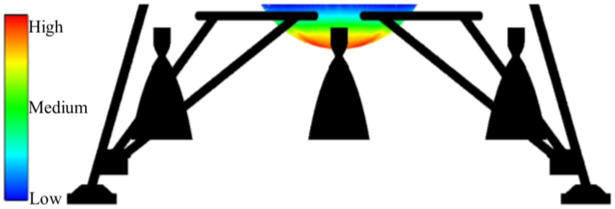

Fig.21. Surface incident radiation contour for 50N bracket, (W/m^2)

Figure 22 displays the overall surface incident load over the lander structure. It shows all radiation exposed surfaces, which have to be suitably covered with thermal protection system.

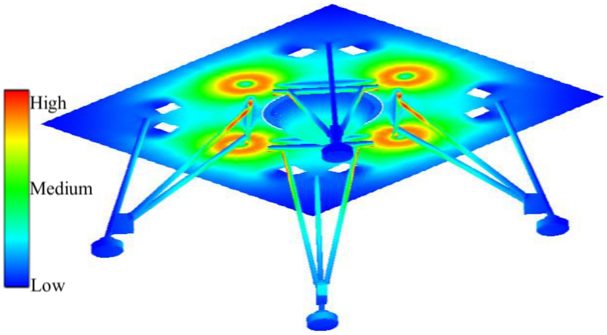

Fig.22. Surface incident radiation contour for 50N bracket, (W/m^2)

3.2.2 Plume Impingement &Convective Heat Load on Lander Structures

3.2.2.1 Plume Impingement

Density Iso surface (1.5e-05 kg/m^3) contour is plotted to capture plume impingement. Figure 23 shows velocity magnitude 3D map, which shows constant density gas moving upwards and impinging the base plate. The same density flow is seen to impinge on foot pad structure of lander legs. The foot pad structure is also seen to be influenced by low density plume gas.

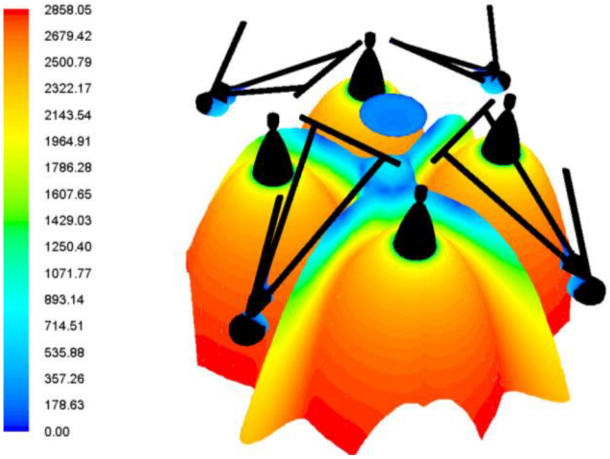

Fig. 23.Density Iso Surface: Velocity 3D map

Two dimensional representation of plume impingement on lander legs is also estimated and is presented in Fig. 22 and Figure 23. Figure 24 presents velocity magnitude Iso-curve showing gas plume, hitting the lander leg assembly. It shows that only shear layer of plume is hitting lander legs with velocity less than 250m/s. Figure 25 shows temperature Iso-curve with plume gas hitting lander legs. Temperature profile shows a zone of 490K gas near the lander legs. This part of plume hitting lander legs will directly contribute towards convective heating of lander legs. The density of gas impinging on lander leg structure is very low (in order of 1.5e-05 kg/m^3), which may not lead to significant convective heat load on these structures

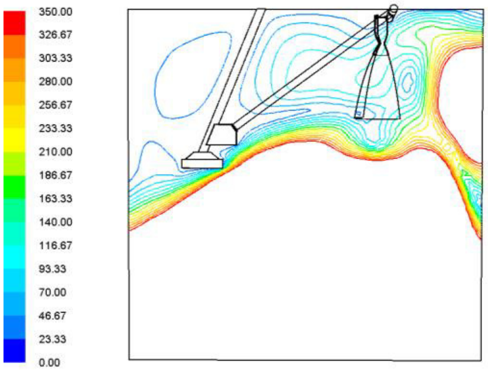

Fig.24. Velocity magnitude Iso-curve near to lander legs, (m/s)

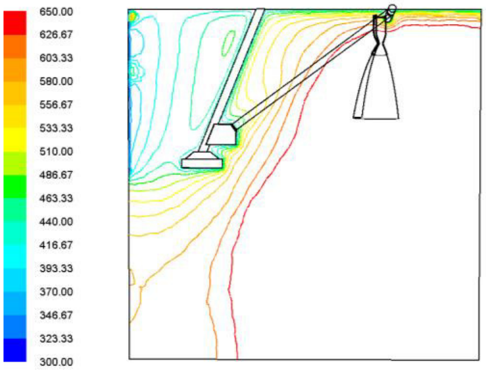

Fig.25. Temperature Iso-curve near to lander legs, (K)

3.2.2.2 Convective Heat Flux Estimation

A similar pattern as incident radiation was seen for convective flux on base plate. Figure 26 displays the convective flux on base plate with maximum value near 800N thrusters, which is primarily due to combined effect of high temperature recirculating entrapped gas near to throat and updraft plume.

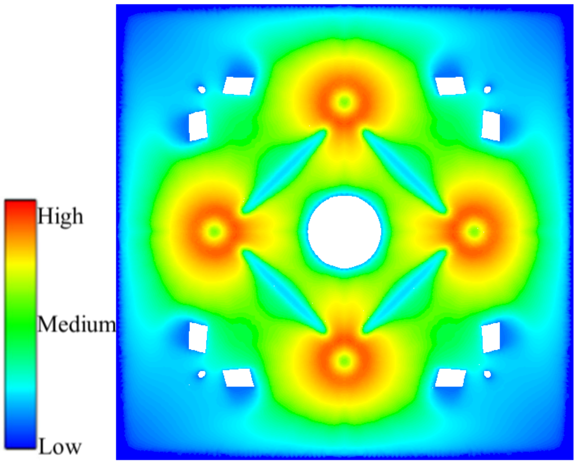

Fig.26. Convective heat flux contour of base plate, (W/m^2)

The outer periphery of base plate is seen at lower value of convective heat flux, with regions loosing heat outside.

Lander leg structure experience high convective flux in comparison to base plate due to proximity to thruster plume. A similar pattern like incident radiation is observed for convective heat flux on lander leg assembly as shown in Fig. 27. It shows heating of lander legs in the region near to plume, whereas as a local maxima was seen on stiffener leg which is due to direct plume impingement from 50N thruster plume.

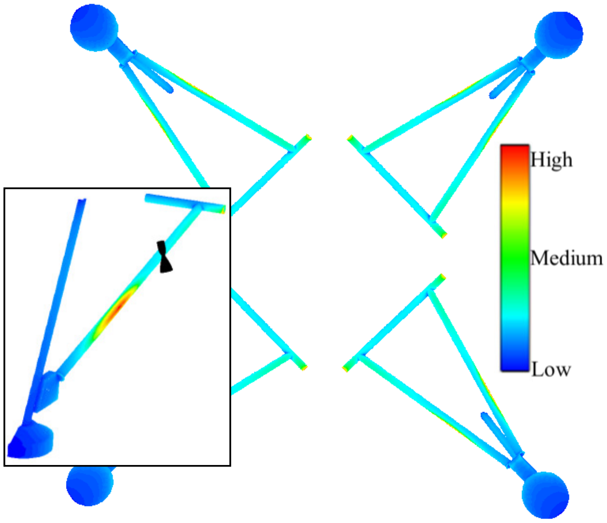

Fig.27. Convective heat flux contour of lander legs (bottom view), (W/m^2)

A combined study was done with steady operation of 50N thruster with plume flow of 800N engine. Figure 28 shows the snapshot of velocity magnitude of 50N thruster in presence of 800N engine plume. An insignificant change in 800N plume flow field was observed during firing of 50N AOCS thruster. The steady operation of 50N thruster was seen to impose high localized convective load on lander leg which is in proximity of 50N thruster. Figure 29 shows the top view and front view of lander leg exposed to high impingement heat flux of 50N thruster plume.

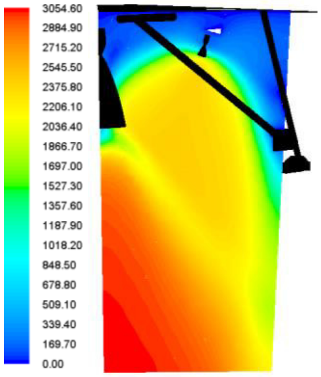

Fig.28. Velocity magnitude for 50N thruster

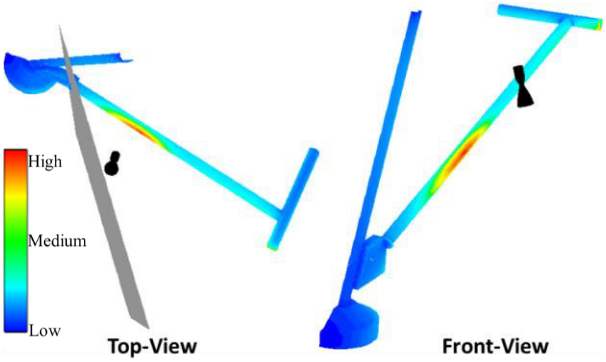

Fig.29. Convective heat flux contour of lander leg (top-view),(W/m^2)

A similar pattern like incident radiation is observed for convective heat flux on 50N bracket. Figure 30 presents the intensity of convective load on 50N support bracket. A localized maxima is observed near the nozzle throat, which is due to circulation of high temperature gas near the 50N thruster.

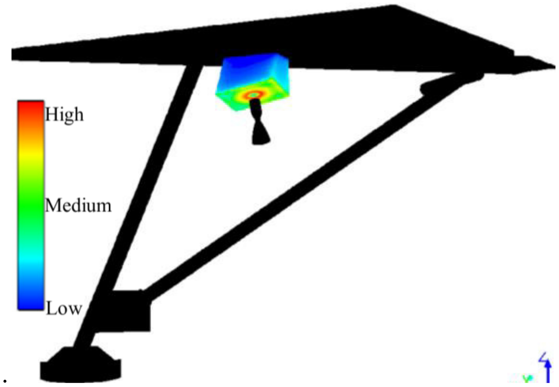

Fig.30. Convective heat flux contour for 50N bracket.

A detailed study was carried out to understand the flow features and associated thermal loads on Chandryaan-2 lander. Plume impingement and convective loads on the structure are estimated, which will be used for design of appropriate protection system during full operation of Chandrayyan-2 lander during soft landing.

5. Conclusion

CFD study is carried out for clustered 4 nozzle configuration of 800N thrusters under simultaneous firing during braking phase of Chandrayaan-2 mission. Plume-plume interaction is observed to initiate at an axial location of 0.2 m from the thruster nozzle exit. The interaction of plumes results in high static pressure and temperature zones. Entrainment zone is observed to form between 4 engines, which is due to high static pressure at the interaction plane and resultant updraft plume. Surface incident radiative and convective heat flux on the base plate and lander leg structure is estimated for appropriate design of thermal protection of lander. The magnitude of convective heat load on lander structures was seen to be lower than radiative heat flux due to low plume density. Incident and convective heat flux plots indicated that, nozzle throat will act as the main source of radiative and convective heating of lander components, with minor contribution from updraft plume.

5. References

[1].Base Heating Sensitivity Study for a 4-Cluster Rocket Motor Configuration in Supersonic Freestream, *Mehta M., Canabal F., et. al.,* NASA Thermal and Fluids Analysis Workshop, 2011.

[2].Numerical Analysis of Base Flow-field at High Altitude for a Four-Engine Clustered Nozzle Configuration, *Wang, T.S.*, AIAA-93-1923

[3].Base Flow and Heat Transfer Characteristics of a Four-Nozzle ClusteredRocket Engine: Effect of Nozzle Pressure Ratio R. Nallasamy and M. Kandula, AIAA

[4].ANSYS FLUENT v.15 Registered

[5].Sarkar S, Erlebacher G &Husaaini M Y, J Fluid Mech. 227 (1991) 473

Acknowledgements

Authors express their sincere gratitude to the Director, LPSC and the Project Team-Chandrayaan-2 at LPSC and ISAC to carry out this work successfully.